European Journal of Mechanics A/Solids 55 (2016) 278–288

Contents lists available at ScienceDirect

European Journal of Mechanics A/Solids

journal homepage: www.elsevier.com/locate/ejmsol

A rate-independent crystal plasticity model with a smooth elastic–plastic transition and no slip indeterminacy

Samuel Forest [a, *], M.B. Rubin [b]

[a] Mines ParisTech CNRS Centre des Matériaux UMR 7633, BP 87 91003 Evry, France
[b] Faculty of Mechanical Engineering, Technion–Israel Institute of Technology, 32000 Haifa, Israel

ARTICLE INFO

Article history:
Received 3 May 2015
Accepted 30 August 2015
Available online 25 September 2015

Keywords:
Rate-independent crystal plasticity
Slip system
Smooth elastic–plastic transition

ABSTRACT

A new crystal plasticity constitutive model is proposed that combines, for the first time, the following features: (*i*) multi-criterion formulation, (*ii*) exact strain rate-independence, (*iii*) absence of a consistency condition and (*iv*) smooth elastic–plastic transition. It is characterised by the existence of a rate-independent overstress that removes the usual possible indeterminacy of simultaneously activated slip systems. The performance of the new model compared to a reference crystal plasticity model by Méric and Cailletaud (1991) in its quasi-rate-independent limit was evaluated in the case of two significantly different materials, namely single crystalline copper and a nickel-based superalloy at room temperature. The provided material point simulations of complex loading paths and large scale finite element simulations do not show any spurious effect of the model, provided that the overstress remains small enough. The improved computational efficiency of the model is discussed.

1. Introduction

There is a need for rate-independent single crystal plasticity models in many applications for the deformation of FCC single crystals like copper and aluminium and other engineering materials close to room temperature. The well-established Schmid criterion governing the activation of plastic slip systems in many crystals leads to a fundamental indeterminacy in the case of some multi-slip configurations as discussed by Bishop and Hill (1951) and explored by Renouard and Wintenberger (1976) in the case of perfect plasticity. This is due to the existence of corners and edges in the multi-criterion yield function. Mandel (1965) demonstrated that this ambiguity pertains in the presence of strain hardening. Several combinations of slip systems exist that can accommodate a prescribed overall plastic deformation rate. Criteria are then needed for the selection of active sets of slip systems for instance based on a maximum dissipation principle (Fortunier, 1989; Patoor et al., 2006). Such criteria are generally not sufficient to restore uniqueness of the rate problem.

A viscoplastic regularization was proposed by Hutchinson (1976) where the slip rate is an explicit power law function of the stress and hardening variables. The thermodynamics and physics of such more general viscoplastic laws based on thermal activation theory were settled by Kocks et al. (1975). Combined with a threshold function introducing a purely elastic domain, this class of elastoviscoplastic models has become standard in crystal plasticity simulations (Roters et al., 2010). Quasi-rate independent predictions are then obtained in the limit of vanishing viscous stress contribution. This limiting case was analyzed for complex multiaxial loading paths and for a wide range of constitutive frameworks by Busso and Cailletaud (2005).

An alternative to viscoplastic regularization to obtain a truly rate-independent single crystal plasticity criterion is to use a single yield function of all resolved shears stresses and build a yield surface with rounded corners. It is based on the use of an exponent n such that the multicriterion Schmid law is retrieved for infinite values of n, see (Arminjon, 1991; Gambin, 1991, 1992; Schurig and Bertram, 2003). This approach was successfully applied to the deformation of polycrystals by Darrieulat and Piot (1996), Montheillet et al. (1985), to the simulation of texture evolution (Gambin and Barlat, 1997) and, more recently, to ductile fracture of single crystals (Paux et al., 2015). The drawback of this single criterion formulation is that it is more difficult to introduce interaction between slip systems and latent hardening effects.

Pragmatic mathematical solutions to the uniqueness problem were proposed using the notion of a generalized inverse used as an active set selection method by Anand and Kothari (1996), Miehe

* Corresponding author.
E-mail addresses: samuel.forest@ensmp.fr (S. Forest), mbrubin@tx.technion.ac.il (M.B. Rubin).

http://dx.doi.org/10.1016/j.euromechsol.2015.08.012
0997-7538/

et al. (1999). The performance of such regularizations was also analysed in Busso and Cailletaud (2005).

Another long-standing problem of plasticity theory is the design of rate-independent elastoplasticity models with a smooth elastic–plastic transition. Usual models ensure continuity of the stress evolution at yielding but not its differentiability. Lubliner et al. (1993) developed a rate-independent overstress model (Malvern, 1951; Perzyna, 1970) with a finite elastic range and a smooth elastic–plastic transition. Einav (2012) generalized previous hypoplastic and hyper-plastic models which produce rate-independent smooth stress–strain curves with no elastic range. More recently Hollenstein et al. (2013, 2015) developed a large deformation model (denoted by HJR) for both rate-independent and rate-dependent material response with a finite elastic range and a smooth elastic–inelastic transition. Specifically, a rate-independent overstress model can be obtained by replacing the standard plastic multiplier with the norm of the total rate of distortional deformation.

The objective of the present work is to propose and validate the first single crystal plasticity model combining the following features: (*i*) multi-criterion formulation, (*ii*) exact rate-independence, (*iii*) absence of a consistency condition and (*iv*) smooth elastic–-plastic transition. For that purpose, the HJR model Hollenstein et al. (2013) is combined with the well-established simple elastoviscoplastic single crystal model by Méric et al. (1991), Méric and Cailletaud (1991). It is emphasized that multi-criterion crystal plasticity models based on an overstress viscoplastic formulation can easily be modified in the same way to obtain a rate-independent smooth elastic–plastic transition. This is done by modifying the functional form of the rate of plastic slip on each slip system with no change to other parts of the constitutive formulation. In particular the hardening laws, including interaction between slip systems, are left unchanged.

An outline of this paper is as follows. The initial and modified models are formulated in Section 2 within the isothermal small strain framework. An extension to finite deformation crystal plasticity is presented in Section 2.3. Two physically relevant cases of rate-independent single crystal materials are selected for the validation of the new model with respect to reference results. Copper single crystal behaviour at room temperature is well-established and material parameters for various single crystal models are available in literature for the comparison. Single crystalline copper displays a very low initial critical resolved shear stress followed by very strong strain hardening. In contrast, Nickel-base superalloys at room temperature exhibit a high yield stress and low hardening. The responses of both models to homogeneous simple and complex loading paths are compared for copper in Section 3. Non-homogeneous conditions are simulated by means of the finite element method to evaluate the performance of the new model for structural computations. The case of a double-notched single crystal superalloy specimen is investigated in Section 4. In all cases, the role of the overstress, the physical relevance of the model response and computational efficiency are investigated.

Regarding notations, all vectors and higher order tensors are boldface. The second order unit tensor is $\boldsymbol{I}$ and $\boldsymbol{A}\cdot\boldsymbol{B} = \mathrm{tr}(\boldsymbol{A}\boldsymbol{B}^T)$ is the inner product of 2 s order tensors $\boldsymbol{A}$,$\boldsymbol{B}$. The Macaulay brackets <–> are applied to scalars and denote the ramp function.

2. Model formulation

2.1. Small strain formulation

Single crystal metals and alloys endowed with N plastic slip systems, each characterised by the slip system direction $\boldsymbol{\ell}^s$ and the normal to the slip plane $\boldsymbol{n}^s$, are considered. The strain tensor is partitioned into the elastic and plastic contributions:

$$\boldsymbol{\varepsilon} = \boldsymbol{\varepsilon}^e + \boldsymbol{\varepsilon}^p \tag{1}$$

The elastic strain tensor is related to the stress tensor by Hooke's law

$$\boldsymbol{\sigma} = \boldsymbol{C}\boldsymbol{\varepsilon}^e \tag{2}$$

where $\boldsymbol{C}$ denotes the generally anisotropic fourth rank tensor of elastic moduli. The plastic strain rate results from the slip processes with respect to all slip systems,

$$\dot{\boldsymbol{\varepsilon}}^p = \sum_{s=1}^{N} \dot{\gamma}^s \left(\boldsymbol{\ell}^s \otimes \boldsymbol{n}^s + \boldsymbol{n}^s \otimes \boldsymbol{\ell}^s\right)/2 \tag{3}$$

where the amount of slip rate on each slip system is denoted by the variable $\dot{\gamma}^s$. Note that in crystal plasticity, the slip direction is contained in the slip plane so that plastic strain rate is deviatoric.

The driving force for plastic slip on slip system s is the resolved shear stress

$$\tau^s = \boldsymbol{\sigma}\cdot\left(\boldsymbol{\ell}^s \otimes \boldsymbol{n}^s\right) \tag{4}$$

The yield criterion is a generalization of Schmid's law involving scalar hardening variables x^s and r^s (Méric et al., 1991):

$$f^s(\boldsymbol{\sigma}, x^s, r^s) = |\tau^s - x^s| - r^s \tag{5}$$

In this function, r^s denotes the critical resolved shear stress whereas x^s is a scalar back-stress characterizing the centre of the elastic range in the one-dimensional space of resolved shear stresses. There are N such elastic ranges. Plastic slip can occur only if the function f^s becomes positive. The viscoplastic flow rule, initially proposed in Méric et al. (1991), is specified in terms of the viscosity parameters, K and n,

$$\dot{\gamma}^s = \left\langle \frac{f^s}{K} \right\rangle^n \mathrm{sign}(\tau^s - x^s) \tag{6}$$

Motivated by the HJR model by Hollenstein et al. (2013), the main idea of this paper is to replace the rate of slip on each slip system with a rate-independent formulation of the form

$$\dot{\gamma}^s = \dot{e}\left\langle \frac{f^s}{R} \right\rangle \mathrm{sign}(\tau^s - x^s), \tag{7}$$

where R is a positive constant having the units of stress and $\dot{\boldsymbol{e}}$ is a non-negative homogeneous function of order one in the total strain rate $\dot{\boldsymbol{e}}$. For the simplest model, $\dot{\boldsymbol{e}}$ is taken to be the total equivalent distortional strain rate

$$\dot{e} = \sqrt{\frac{2}{3}\dot{\boldsymbol{e}}'\cdot\dot{\boldsymbol{e}}'}, \quad \dot{\boldsymbol{e}}' = \dot{\boldsymbol{e}} - \frac{1}{3}(\dot{\boldsymbol{e}}\cdot\boldsymbol{I})\boldsymbol{I}, \tag{8}$$

where $\dot{\boldsymbol{e}}'$ is the deviatoric part of the total strain rate tensor $\dot{\boldsymbol{e}}$. Since the rate of inelasticity (7) is linear in the total equivalent strain rate $\dot{\boldsymbol{e}}$ all evolution equations in the proposed theory are homogeneous of order one in time so they characterize a rate-independent response. Furthermore, the rate of inelasticity (7) is used for all states so there is no need for special treatment of loading and unloading conditions.

Also, in order to take full advantage of previous developments, the functional form for f^s and the evolution equations for x^s and r^s remain unchanged. The value of R in (7) replaces K in (6) as a new

calibration constant. This constant can be determined by matching a single uniaxial stress–strain curve.

This new crystal plasticity model is called the Smooth Rate Independent Crystal plasticity model, in short SRIX, in the following.

A generalization of (7) could be to replace $\dot{\boldsymbol{\varepsilon}}$ by the magnitude $\dot{\varepsilon}^s$ of the total strain rate projected on the slip system as

$$\dot{\varepsilon}^s = |\dot{\boldsymbol{\varepsilon}} \cdot \boldsymbol{\ell}^s \otimes \boldsymbol{n}^s| \tag{9}$$

However this would introduce additional anisotropy in the constitutive equations which would need to be examined in future work.

For each slip system, the cumulative slip variable, v^s, is defined by the following evolution equation:

$$\dot{v}^s = |\dot{\gamma}^s| \tag{10}$$

The evolution equations for the hardening variables, x^s and r^s, are taken from Méric et al. (1991), Busso and Cailletaud (2005) without modification. The critical resolved shear stress is an explicit function of the cumulative slips:

$$r^s = \tau_c + Q \sum_{q=1}^{N} h^{sq}(1 - \exp(-bv^q)) \tag{11}$$

where the material parameters Q and b characterize the nonlinear hardening for each slip system. The interaction matrix h^{sq} introduces self and latent hardening among the slip systems (Mandel, 1965). Moreover, the back-stress evolution law

$$\dot{x}^s = C\dot{\gamma}^s - Dv^s x^s \tag{12}$$

depends on two material parameters, c and d, and leads to nonlinear kinematic hardening.

The thermodynamical consistency of the reference model was established in Besson et al. (2009), Busso and Cailletaud (2005) by a proper choice of state and internal variables. The new formulation departs from the reference model only in the expression of the plastic multiplier. As a consequence, positivity of the dissipation rate is ensured for all processes, for the same reasons as in Besson et al. (2009). The thermodynamical formulation is not recalled here for the sake of brevity.

2.2. Characterization of the overstress in tension

Under plastic loading condition, the resolved shear stress with respect to each slip system can be expressed in terms of three contributions deduced from the new flow rule (7):

$$\tau^s = \pm r^s \pm R\frac{|\dot{\gamma}^s|}{\dot{\varepsilon}} + x^s \tag{13}$$

where the sign of the first two terms is given by that of $\tau^s - x^s$. The first contribution on the right-hand side includes the initial critical resolved shear stress and subsequent isotropic hardening. The second one is a rate-independent overstress with magnitude controlled by parameter R. The last one denotes slip system based kinematic hardening.

An analytical solution of the tension test for a single crystal can be worked out for the present SRIX model in the absence of hardening ($Q = C = 0$). It is provided in Appendix A in the case of tension in the direction [001]. The solution predicts a smooth nonlinear evolution of quasi-exponential type with a limit stress value equal to

$$\sigma_{33}^{\infty} = \sqrt{6}\tau_c(1 + O_R), \quad O_R = \frac{\sqrt{6}}{8}\frac{R}{\tau_c} \tag{14}$$

where O_R is the overstress ratio in the present SRIX model. The tensile direction is the direction 3 of the Cartesian coordinate frame. It confirms that for vanishing values of R, the present SRIX model coincides with the classical Schmid law.

In the reference model, the tensile test along [001] can also be solved and leads to the following expression of a limit stress in the absence of hardening

$$\sigma_{33}^{\infty} = \sqrt{6}\tau_c(1 + O_V), \quad O_V = \left(\frac{\sqrt{6}\dot{\varepsilon}_{33}}{8}\right)^{1/n}\frac{K}{\tau_c}, \quad \dot{\varepsilon}_{33} > 0 \tag{15}$$

where the overstress ratio O_V is rate-dependent.

It then follows that the axial stress predicted by both models will be the same for a specified axial strain rate when

$$R = \frac{8}{\sqrt{6}}K\left(\frac{\sqrt{6}\dot{\varepsilon}_{33}}{8}\right)^{1/n} \tag{16}$$

The expression (16) is used in Sections 3 and 4 to determine a constant value of R which causes the present SRIX model to have the same overstress as the standard viscoplastic model at a *specified* representative equivalent total strain rate.

2.3. Proposed finite deformation extension

A straightforward extension of the previous model to finite deformation crystal plasticity is presented. According to standard crystal plasticity, a multiplicative decomposition of the deformation gradient, $\boldsymbol{F}$, into elastic and plastic contributions is adopted

$$\boldsymbol{F} = \boldsymbol{E}\boldsymbol{P} \tag{17}$$

whereby an intermediate isoclinic local configuration is defined according to Mandel (1973). The plastic deformation is determined by the flow rule in the form

$$\dot{\boldsymbol{P}}\boldsymbol{P}^{-1} = \sum_{s=1}^{N} \dot{\gamma}^s \boldsymbol{\ell}^s \otimes \boldsymbol{n}^s \tag{18}$$

from which Eq. (3) is the linearized version. Note that alternative formulations of the finite deformation anisotropic elastoplasticity theory exist that do not directly make use of a multiplicative decomposition (Bertram, 1999; Rubin, 1994, 2012), but the standard presentation is sufficient for the purpose of the present work.

The same yield functions (5) can be used for viscoplastic single crystals at finite deformation, provided that the resolved shear stress is computed according to the following projection:

$$\tau^s = \boldsymbol{M} \cdot (\boldsymbol{\ell}^s \otimes \boldsymbol{n}^s), \quad \text{with} \quad \boldsymbol{M} = (\det \boldsymbol{E})\boldsymbol{E}^T\boldsymbol{\sigma}\boldsymbol{E}^{-T} \tag{19}$$

where $\boldsymbol{\sigma}$ and $\boldsymbol{M}$ respectively are the Cauchy stress tensor and the Mandel stress tensor (Haupt, 2000).

In the large deformation formulation, the slip rate $\dot{\gamma}^s$ in Eq. (7) is specified in the form (6) where the equivalent total distortional strain rate $\dot{\boldsymbol{\varepsilon}}$ is defined in terms of the deviatoric part $\boldsymbol{D}'$ of rate of deformation tensor $\boldsymbol{D}$

$$\dot{\varepsilon} = \sqrt{\frac{2}{3}\boldsymbol{D}' \cdot \boldsymbol{D}'} \tag{20}$$

where $\boldsymbol{D}$,$\boldsymbol{D}'$ are defined in terms of the velocity gradient $\boldsymbol{L}$ by

$$\boldsymbol{L}=\frac{\partial \boldsymbol{v}}{\partial \boldsymbol{x}}=\dot{\boldsymbol{F}}\boldsymbol{F}^{-1},\quad \boldsymbol{D}=\frac{1}{2}\left(\boldsymbol{L}+\boldsymbol{L}^{T}\right),\quad \boldsymbol{D}'=\boldsymbol{D}-\frac{1}{3}(\boldsymbol{D}\cdot\boldsymbol{I})\boldsymbol{I} \tag{21}$$

The same hardening variables, r^s and x^s, and corresponding evolution laws as in the previous subsection can be used.

3. Application to the cyclic behaviour of single crystalline copper

3.1. Material parameters

The Méric–Cailletaud single crystal plasticity model (Méric et al., 1991) is used as the reference model to assess the main features of the SRIX model. Material parameters of the reference model have been identified for copper single crystals under cyclic loading in several publications including (Méric et al., 1993; Šiška et al., 2007a; Musienko et al., 2007; Šiška et al., 2007b, 2009). The parameters retained for the numerical simulations of this work are taken from the last reference and are given in Table 1. They were identified from experimental results including monotonic and cyclic tests performed on OFHC copper for various crystallographic directions, see (Méric et al., 1993). The components of the interaction matrix h^{ij} are close to those proposed by Franciosi (1985). Specifically, the diagonal components of h^{ij} are all equal to 1 and its off-diagonal components are all equal to the latent hardening parameter $h=1.4$. Copper is a FCC crystal at room temperature. The twelve octahedral slip systems {111}<110> are taken into account in the simulations. Anisotropic elasticity is required for copper with three independent cubic moduli: $C_{11}=159.3$ GPa, $C_{12}=122$ GPa, $C_{44}=81$ GPa, after El Houdaigui et al. (2007).

The material parameters used for the present SRIX model are the same as those for the reference model, except that parameter R replaces K. The value of R is chosen in such a way that both models provide the same overstress for a tensile test along [001] at a given strain rate. The viscous overstress predicted by the reference model is deduced from formula (15). The values of the overstress factor O_V are given for several strain rates in Table 2 ranging from to 10^{-7} to 10^{-1} s^{-1}. Thus, it can be seen that the reference model predicts only a small overstress. The value $R=0.2$ MPa is chosen for the following simulations. This value provides an overstress close to the viscous stress reached in tension at a strain rate of 10^{-4} s^{-1}. These material constants are recorded in Table 1. The impact of different values of R in the SRIX model will be explored in Section 3.2.

The tensile responses of single copper along 4 distinct lattice directions are simulated by means of both models and are shown in Fig. 1. As expected, the [111] direction provides the strongest response. It is associated with the simultaneous activation of 6 slip systems sharing the same amount of slip γ for symmetry reasons. In contrast, the lowest curve, obtained for tension along [123], first triggers one single slip system and then two additional ones due to strain hardening. It is well-known that copper exhibits very strong hardening reaching high stresses compared to the small initial critical resolved shear stress $\tau_c=1.8$ MPa.

Table 1
Material parameters for single crystalline copper and Nickel-base superalloy PWA1489 for the reference and SRIX models.

Reference copper	n 10	K (MPa$^{1/n}$) 0.2	τ_c (MPa) 1.8	Q (MPa) 6	b 15	h 1.4	C (MPa) 4500	D 600
SRIX copper	–	R (MPa) 0.2	τ_c (MPa) 1.8	Q (MPa) 6	b 15	h 1.4	C (MPa) 4500	D 600

Reference PWA1489	n 15	K (MPa$^{1/n}$) 4	τ_c (MPa) 324	H (MPa) 75	h 0
SRIX PWA1489	–	R (MPa) 9	τ_c (MPa) 324	H (MPa) 75	h 0

Table 2
Viscous stress arising in the reference model for a single crystal in tension along [001] and associated value of parameter R in the SRIX model leading to the same value of the overstress at the given strain rate. The material parameters for both models and two materials are taken from Table 1.

$\dot{\varepsilon}_{33}$ (s^{-1})	O_V copper	R (MPa) copper	O_V PWA1489	R (MPa) PWA1489
10^{-7}	0.0197	0.116	0.0039	4.122
10^{-5}	0.0312	0.184	0.0053	5.604
10^{-3}	0.0495	0.291	0.0072	6.533
10^{-2}	0.0622	0.366	0.0084	8.821
10^{-1}	0.0784	0.461	0.0098	10.355

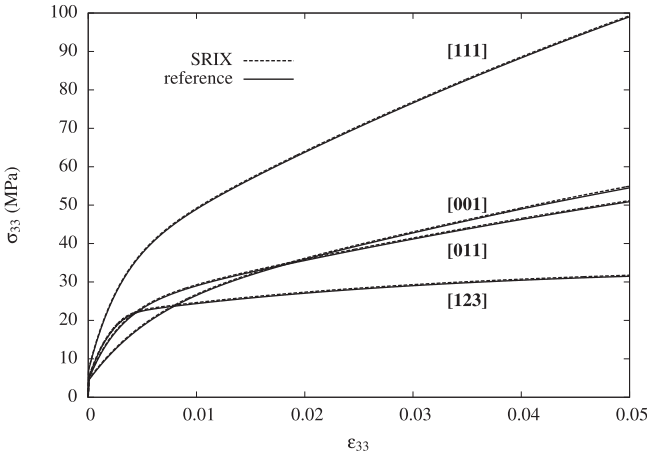

Fig. 1. Tensile responses of the reference crystal plasticity and SRIX models along four distinct lattice directions ($\dot{\varepsilon}_{33}=5\times10^{-5}$ s^{-1}). The material parameters are given in Table 1.

It is apparent that the reference and SRIX models predict practically the same material response in tension, for the considered material parameters of Table 1. This means that the new model can replace the original one without altering material behaviour.

The same holds true for the case of cyclic loading, as shown in Fig. 2 for two crystallographic orientations. The curves illustrate the role of kinematic hardening embodied by the material parameters C,D.

3.2. Influence of the parameter R

The specific features of the SRIX model are investigated in the present subsection and in the next one. In particular the values of parameter R are now varied to assess their impact on the material response.

Considering higher values of R leads to a larger overstress and departure from the reference curve. It can be said that the overstress corresponding to the values of the SRIX material parameters from Table 1 leads to negligible overstress.

The same observations are made regarding the cyclic response illustrated in Fig. 3(a). Note that higher values of R lead to smoother elastic–plastic transition on the first loading branch. The Fig. 3(b) shows that the value $R=20$ MPa leads to the activation of the same three slip systems as in the reference case but with a smaller amount of activation for the most activated slip system and a larger amount of activation for the less activated ones, as expected in the presence of larger overstress.

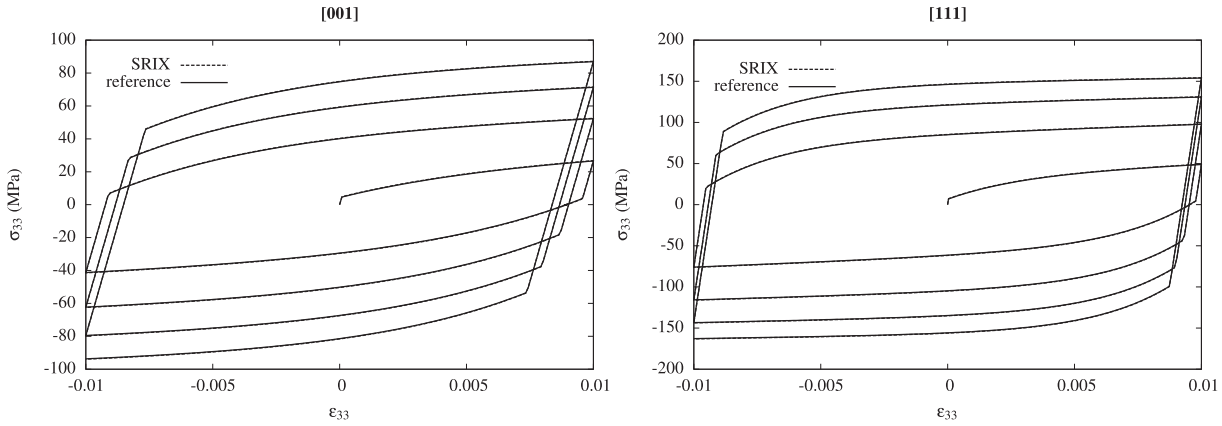

Fig. 2. Cyclic uniaxial responses of the reference crystal plasticity and SRIX models along two distinct crystal lattice directions indicated above each picture. Four cycles with controlled strain amplitudes $\varepsilon_{33} = \pm 0.01$ ($|\dot{\varepsilon}_{33}| = 10^{-3}$ s^{-1}). The material parameters are given in Table 1.

The computational efficiency of the present SRIX model is now compared to that of the reference one. For that purpose, a homogeneous cyclic simple shear test is considered where all strain components are prescribed so that the efficiency of the numerical integration method can be tested independently of the finite element features. A second order Runge-Kutta method is used with automatic time stepping to integrate the constitutive equations, see Besson et al. (2009) for the details of the implementation. Validation of the implementation was performed with respect to the analytical solution of the tensile test considered in Appendix A. The CPU time for the integration part of the code is given in Table 3 for a 4-core Intel-i7 processor[1] with 16 Go RAM and 1.6 GHz. It shows that the present SRIX formulation is thirty times faster than the reference model when using the material parameters of Table 1. Increasing R also reduces the sharpness of the elastic–inelastic transition and leads to improved computational efficiency.

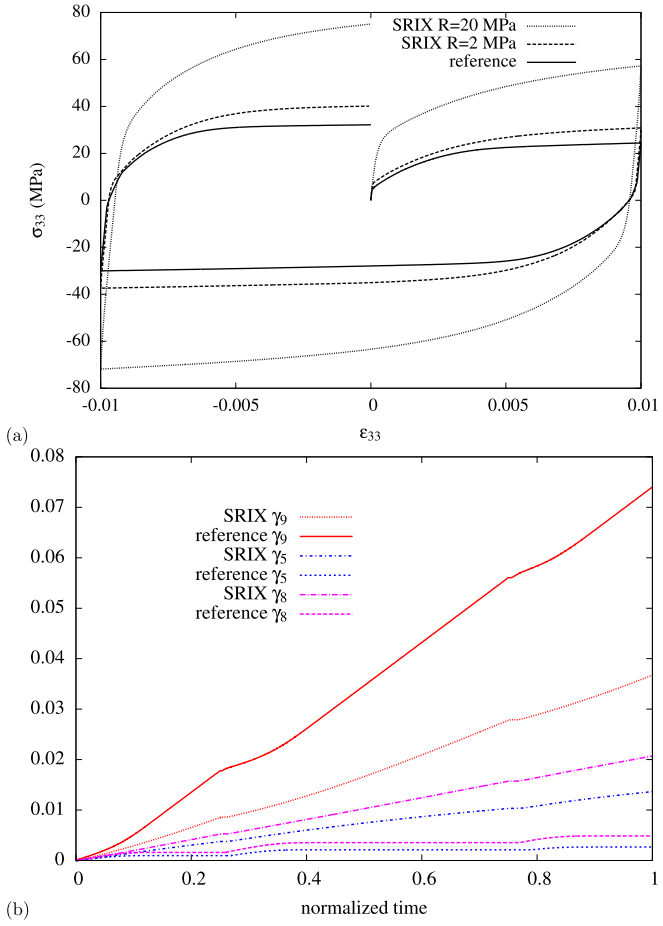

Fig. 3. Cyclic response of the SRIX model in tension–compression along [123] for two different sets of parameters R. (a) Stress–strain loops ($|\dot{\varepsilon}_{33}| = 10^{-3}$ s^{-1}). (b) Amounts of cumulative slip γ_i on the activated slip systems for $R = 20$ MPa. The index i in γ_i refers to the number of the slip system in the list of systems provided in the reference Sabnis et al. (2012). The remaining material parameters are given in Table 1.

Table 3
Elapsed time for the Runge-Kutta numerical integration of the constitutive equations for a cyclic shear test (6 cycles, $\varepsilon_{12} = \pm 1, |\dot{\varepsilon}_{12}| = 2.10^{-3}$ s^{-1} %, crystal orientation [101][010]). Material parameters for the reference computations are those in Table 1.

Copper	Reference	SRIX $R = 0.2$ MPa	SRIX $R = 0.5$ MPa
Integration time (s)	7.5	0.25	0.13
PWA1489	Reference		SRIX $R = 9$ MPa
Integration time (s)	0.62		0.03

3.3. Complex loading paths

The response of the SRIX model is further examined and compared to the reference model for the case of complex loading paths including uniaxial and biaxial cyclic tests. The values of the material parameters used in the simulations are taken from Table 1 for copper. In particular, the parameter R is taken to be 0.2 MPa unless otherwise stated. The following complex loading paths are considered:

- *Small cycles after interrupted tension.*

The tensile test of Fig. 4 was interrupted at $\sigma_{33} = 40$ MPa and followed by stress controlled cycles between $\sigma_{\min} = 36$ MPa and $\sigma_{\max} = 40$ MPa. In the reference model and in the SRIX model when $R = 2$ MPa, these small cycles remain within the elastic domain. In contrast, when $R = 20$ MPa, the present SRIX model predicts a

[1] Intel(R) Core(TM) i7-4600U CPU 2.10 GHz 16 Go DDR3 1600 MHz.

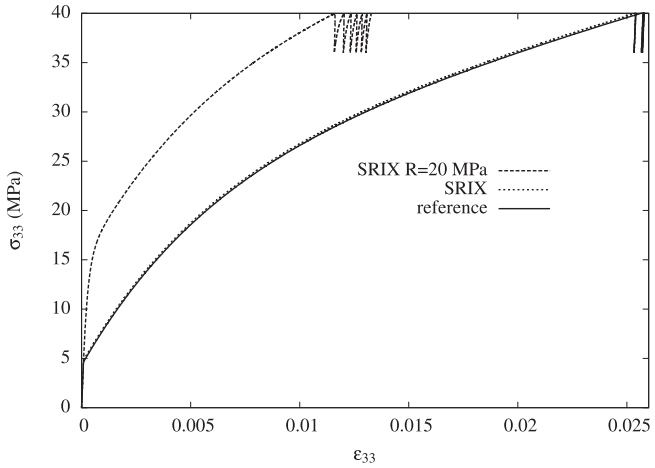

Fig. 4. Tensile test interrupted at $\sigma_{33} = 40$ MPa and followed by six stress controlled cycles with $\sigma_{33}^{min} = 0.9\sigma_{33}^{max}$. Loading direction is [001]. Parameter R is varied and the remaining parameters are given in Table 1.

ratchetting effect due to the existence of a large overstress, as illustrated in Fig. 4.

- *Stress-controlled cyclic test.*

The strong hardening behaviour of copper progressively leads to elastic accommodation when the material is cycled with symmetric stress control, as shown in Fig. 5. No significant difference is observed in the responses of the reference and SRIX models.

- *Strain-controlled test accompanied by mean stress relaxation.* When the strain min and max values are not symmetric, relaxation of the mean stress is observed cycle after cycle until the min and max stress values become symmetric. In this case again, the SRIX and reference models predict the same response, not presented here.
- *Biaxial butterfly test.* A biaxial strain-controlled test is also considered in the analysis although such a test is difficult to perform experimentally on single crystal copper. It combines axial strain prescribed in the direction 3 and shear strain in the 1–2 plane according to a non-proportional *butterfly* path represented in Fig. 6(a). The corresponding stress path in the axial strain/shear strain plane is shown in Fig. 6(b) for the reference and two instances of the SRIX model. The reference simulation shows the complexity of the resulting stress path, namely a strongly distorted butterfly, due to the nonlinearity of the material behaviour and strong work-hardening exhibited by copper single crystals. Note that in the absence of hardening, this test would make it possible to explore the shape of the initial Schmid yield surface. The presence of hardening leads here to unsymmetric increase of the maximal axial and shear stresses during the first cycles. The response of the present SRIX model using the parameters of Table 1 cannot be distinguished from that of the reference model. Increasing parameter R leads to a different response with a non-convex inflexion at the first abrupt change of loading path due to the overstress. The reality of such a material behaviour cannot be assessed from available experimental tests on single crystals.

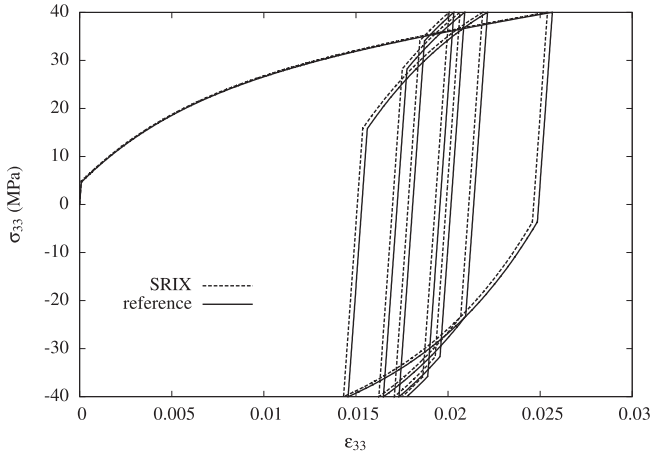

Fig. 5. Cyclic test with controlled stress amplitude $\sigma_{33} = \pm 40$ MPa along the direction [001] ($|\dot{\sigma}_{33}| = 4$MPa.s^{-1}). Four cycles are simulated. The material parameters are given in Table 1.

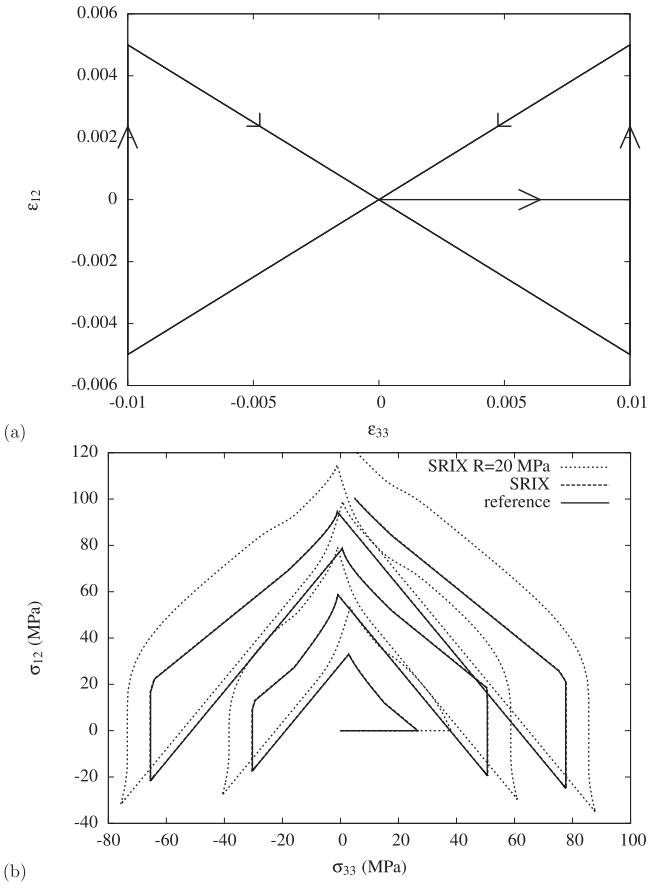

Fig. 6. Biaxial response of the reference and SRIX models. (a) Prescribed loading in the ε_{33}–ε_{12} space (the arrows indicate the loading directions, $|\dot{\varepsilon}_{33}| = 10^{-3}$ s^{-1}, $|\dot{\varepsilon}_{12}| = 5 \times 10^{-4}$ s^{-1}). (b) cyclic stress response. The coordinate axes 1, 2 and 3 respectively coincide with the [100], [010] and [001] axes. Parameter R is varied and the remaining parameters are given in Table 1.

As a conclusion, the simulation of complex loading paths did not reveal any spurious effect of the SRIX model as long as the overstress remains small enough.

4. Application to a single crystal Nickel-base superalloy at room temperature

The performance of the new model is now evaluated in the case of a significantly different material, namely single crystalline

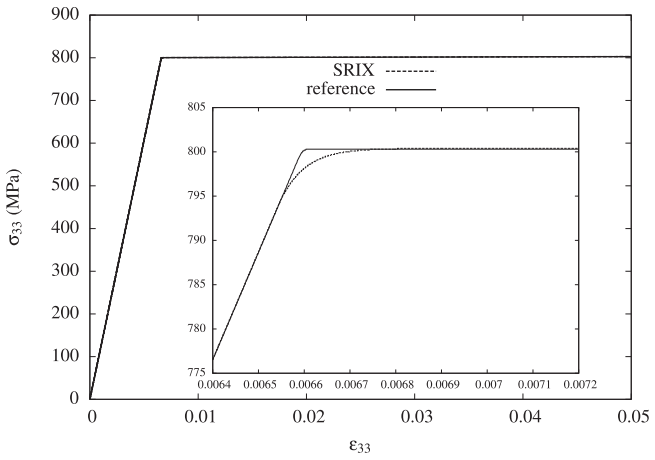

Fig. 7. Tensile curves for PWA1489 along the direction [001] according to the reference and SRIX mode ($\dot{\varepsilon}_{33} = 10^{-2}\ s^{-1}$) with a zoom at the yield point. The material parameters are given in Table 1.

nickel-based superalloy. While copper exhibits a low critical resolved shear stress and very strong hardening, single crystal Nickel-based superalloys display a high yield stress and practically no hardening at room temperature. Their behaviour is notoriously rate-independent at room temperature and therefore it is a good candidate for the use of the present SRIX model. Nickel-based superalloys have a FCC crystal structure like copper.

4.1. Constitutive parameters and tensile behaviour

Material parameters of the reference crystal plasticity model were identified for single crystalline Nickel-base superalloy PWA1489 at room temperature by Sabnis et al. (2012, 2013). Calibration was performed from the tensile curve along [001] that exhibits a high and sharp yield stress and very low hardening represented in the model by quasi-linear hardening with a low slope. Material behaviour is close to elastic-perfectly plastic. The corresponding parameters are given in Table 1. In contrast to copper, linear hardening is used here in the form:

$$r^s = \tau_c + Hv^s \tag{22}$$

which replaces the hardening law (11). The linear hardening modulus is called H. It can be noted that no latent hardening is introduced in the model, $h = 0$. This is a specific feature of single crystalline Nickel-based superalloys, as established experimentally by means of tension–torsion experiments by Nouailhas and Cailletaud (1995). The physical origin of this unusual property compared to standard FCC crystals probably lies in the underlying two-phase microstructure of Nickel-base superalloys characterized by a quasi-periodic network of cuboidal coherent γ'-precipitates embedded in the γ-matrix (Vattré et al., 2010).

Another important feature of single crystalline Nickel-based superalloys is the existence of six effective cubic slip systems in addition to the usual octahedral slip systems. They were observed during the tension of <111>-oriented single crystals by Méric et al. (1991) and corresponding material parameters were identified in the latter work. However, only octahedral slip systems were considered by Sabnis et al. (2012, 2013) and shown to be sufficient to account for the slip line patterns observed in notched single crystals loaded in the <001> direction. Accordingly, the twelve octahedral slip systems are used for PWA1489 in the present work.

Anisotropic elasticity is required for PWA1489 with three independent cubic elastic moduli: $C_{11} = 250$ GPa, $C_{12} = 163$ GPa, $C_{44} = 129$ GPa.

The material parameters K and n of Table 1 were chosen by Sabnis et al. (2012). It is well-known that low values of K, and/or high values of n, are required to limit rate sensitivity in the reference model. On the other hand, numerical integration of the constitutive equations is facilitated by a smoother elastic–viscoplastic transition with associated larger rate-sensitivity. Table 2 shows that viscous overstress induced by the specified values of K and n for PWA1489 is very low. Using formula (16), a value of parameter R in the SRIX model can be identified by equating the overstress values of both models. Here, $R = 9$ MPa so that the reference and SRIX models predict the same tensile curve for the PWA1489 along [001] at a strain rate slightly larger than

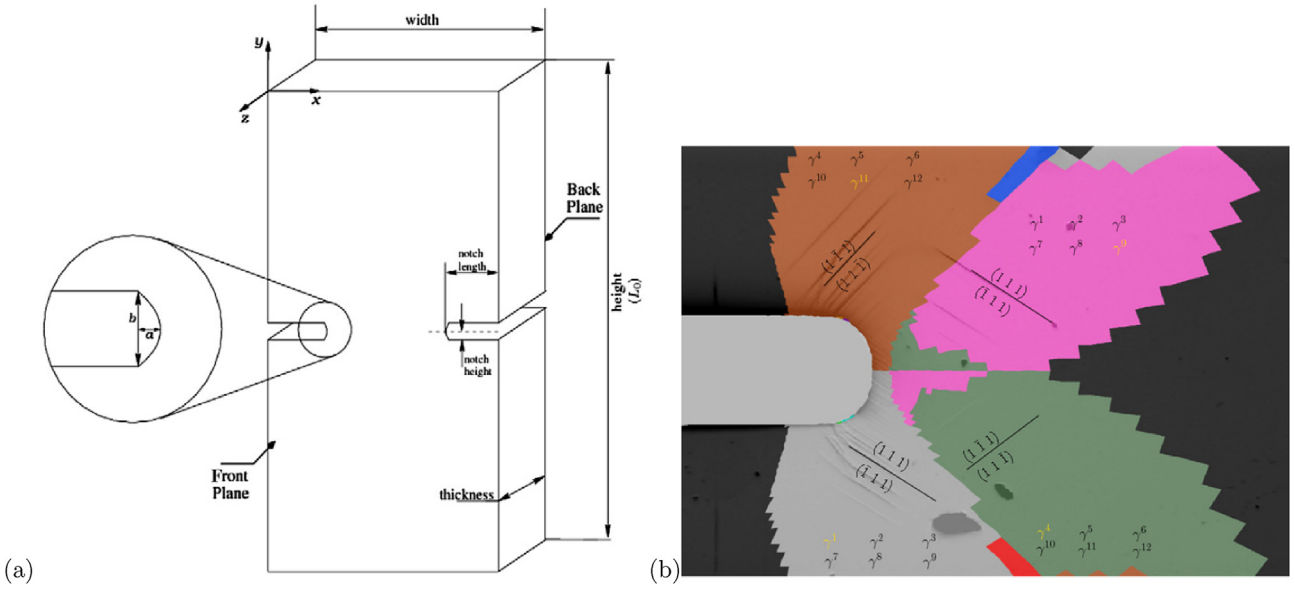

Fig. 8. (a) Geometry of the double-notched single crystal specimen. (b) Slip lines observed at the notch superimposed on the predicted zones of plastic slip activity. After Sabnis et al. (2012).

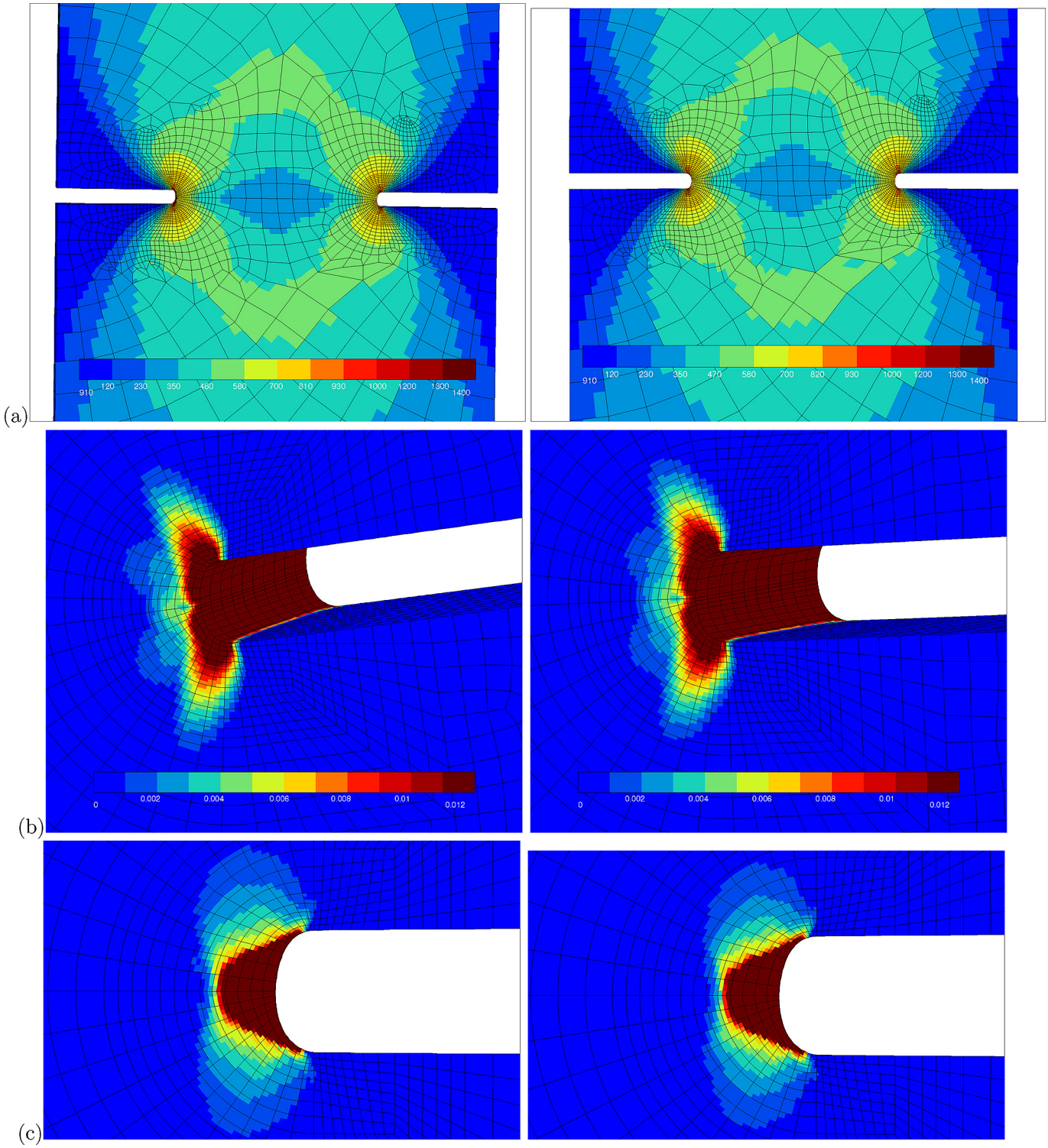

Fig. 9. (a) Von Mises equivalent stress (MPa) maps at the free surface during tension of a double-notched specimen made of PWA1489. Field of cumulative plastic slip $\sum v^s$ at the right notch: (b) at the free surface, (c) in the mid plane of the sample. The left and right pictures correspond to predictions of the reference and SRIX models, respectively.

$\dot{\varepsilon}_{33} = 10^{-2}\ s^{-1}$. The corresponding tensile curves are given in Fig. 7. They are almost superimposed. A small difference is noticed at the yield point which is sharper according to the reference model than for the SRIX model.

The improved numerical efficiency of the present SRIX model compared to that of the reference one was checked for the material parameters of PWA1489 using the same cyclic shear test as in section 3.2. The corresponding elapsed times are given in Table 3. The present SRIX model is found to be twenty times faster than the reference model with the parameters of Table 1.

4.2. Finite element simulation of a notched single crystal specimen

The performance of the present SRIX is now evaluated for a 3D finite element simulation for which reference results are available

from Sabnis et al. (2012). The mode I loading of a double-notched plate specimen is considered in the case of PWA1489 material.

4.3. Geometry, finite element mesh and loading conditions

The geometry of the sample is described in Fig. 8(a). The characteristic dimensions are: *width*: 5.04 mm, *height*: 17.7 mm, *thickness*: 1.82 mm, *right notch length*: 1.39 mm, *right notch height*: 0.084 mm, *right notch radius*: 0.056 mm, *left notch length*: 1.36 mm, *left notch height*: 0.084 mm, *left notch radius*: 0.056 mm. The geometry corresponds to that of the real specimen which was experimentally tested and for which slip band activity at notches was examined in Sabnis et al. (2012). Note that the specimen is slightly non-symmetric with respect to notch length so that a full 3D computation is needed.

The corresponding finite element mesh contains 26,940 elements, 119,575 nodes corresponding to 358,725 degrees of freedom. Quadratic brick elements with reduced integration are used.

The orientation of the sample is such that the loading direction y is parallel to [001] and the direction x is [010], see Fig. 8(a). A displacement of 0.05 mm is applied to the upper surface in 5 s, whereas the lower part is clamped. The required axial force to reach this displacement value was found to be 2532 N.

The problem is solved by means of the implicit finite element code Zset (Z–set package, 2013). Global equilibrium is solved using a Newton-Raphson algorithm. Local integration of constitutive equations at Gauss points is performed by means of a second order Runge-Kutta method with automatic time stepping (Besson et al., 2009). For comparison, the simulation was also carried out using an implicit Newton algorithm (θ-method from Besson et al. (2009)) for the integration of the constitutive equations of the reference model. This method is not available yet for the SRIX model.

4.4. Fields of plastic slip at notches

The physical relevance of the reference single crystal model for the present application is illustrated in Fig. 8(b) where the coloured domain of slip activity are superimposed on the image of the surface of the sample displaying slip lines. It was shown in Sabnis et al. (2012) that the predicted activated slip systems are in good agreement with the observed slip traces. The presence of a notch leads to a complex concentrated stress field that can be decomposed into domains of main slip activity illustrated by the colours of Fig. 8(b). The corresponding stress field is illustrated in the form of von Mises equivalent stress maps in Fig. 9(a). There is practically no difference in the local values predicted by both models with the material parameters of Table 1 for PWA1489. The stress concentration is high enough to trigger slip activity around the notches. The field of cumulative plastic slip $\sum_s v^s$ is shown in Fig. 9(b). It goes through the thickness of the sample and displays a complex pattern on the free surfaces. The 3D computation shows that there is a strong free surface effect with a rapid variation of the fields from the free surface toward the interior. The Fig. 9(a) and (b) show the fields at the free surface for comparison with experimentally measured slip line activity, performed on the free surface by Sabnis et al. (2012). The Fig. 9(c) gives the comparison of the cumulative plastic slip field in the mid section of the CT specimen for both models. Quasi-plane strain conditions are met in most part of the sample. The differences between both models' predictions are very small. The somewhat larger differences observed at the free surface are due to mesh size effects close to the free surface. Thinner elements are needed close to the free surface to better capture the boundary layer effect. Due to the crystallographic orientation of the sample, most plastic activity takes place at a wedge angle of almost ±70–90° w.r.t. the horizontal x-axis at the free surface and at a wedge angle of ±45° in the bulk. No significant difference in the plastic slip field is observed between both calculations. The same was checked for individual slip systems, not presented here.

Table 4
Elapsed CPU time for the finite element simulation of the tension of a 3D notched specimen made of PWA1389 depending on the models and integration methods used.

Model	Integration method	Integration CPU-time (s)	Total CPU-time (s)
Reference	Runge-Kutta	4881	99,690
Reference	θ–method	4263	84,370
SRIX	Runge-Kutta	2646	72,990

The computation time for both models is given in Table 4. The total CPU time of the simulation based on the SRIX model is 15–35% shorter than that using the reference model. However, the simulation is characterized by a significant number of degrees of freedom and large amount of time for global matrix inversion. It is more instructive to compare the time spent for the numerical integration of the system of constitutive differential equations. In that case, the new model is 85% faster than the reference model using the same Runge-Kutta integration method, and still 60% more efficient than the reference model which uses the improved θ-method. The improved CPU efficiency using the present SRIX model is less significant for a large calculation based on implicit integration than in the analyses on a single material point presented in Table 3.

5. Conclusion

An alternative model for rate-independent crystal plasticity has been proposed that combines in a unique way the following features: (*i*) multi-criterion formulation, (*ii*) exact strain rate-independence, (*iii*) absence of a consistency condition and (*iv*) smooth elastic–plastic transition. It was used to replace an existing elastoviscoplastic crystal plasticity model in its quasi-rate-independent limit for the case of two significantly different materials, namely single crystalline copper and a Nickel-based superalloy at room temperature. The present SRIX model is characterized by a single specific material parameter, R, that controls the amplitude

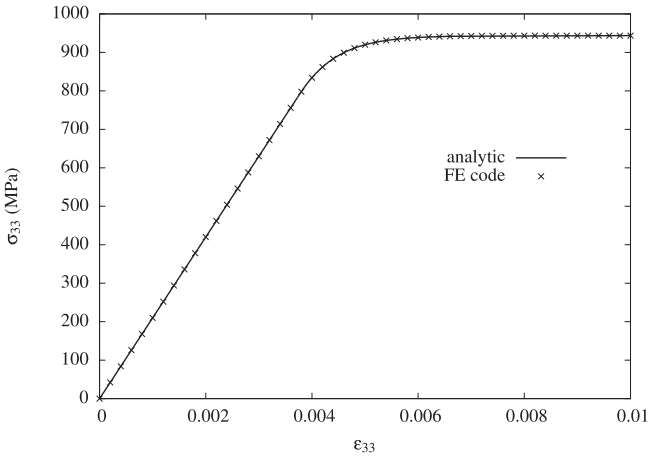

Fig. 10. Analytical vs. numerical solutions of the simple tension of a single crystal in the direction [001]. The following material parameters of the SRIX model were used: $E = 210{,}000$ MPa, ν=0.3, $\tau_c = 324$ MPa, $R = 200$ MPa.

of the rate-independent overstress present in the theory. For small enough values of R, it has been demonstrated that the new model predicts essentially the same material response for various complex loading paths at the material point level or within 3D finite element simulations. No spurious effect could be highlighted in this new formulation compared to the reference model. The main advantage of the present SRIX model is that it can be used to model rate-independent crystal plasticity without arbitrariness of the slip systems and without evaluation of a consistency condition.

The approach, inspired from the HJR model, can be applied to any available crystal plasticity model by introducing a norm of the deviatoric strain rate tensor in the constitutive expression of the slip rate. Variants of this modification can be proposed and should be explored in the future.

Application and validation of the finite strain version of the model remain to be done for forming simulations and crystallographic texture evolution.

The SRIX model has been shown to be computationally more effective than quasi-rate independent viscoplastic crystal plasticity models. The improved CPU efficiency using the SRIX model is less significant for a large finite element calculation based on implicit resolution. However, it is expected that use of the SRIX model in an explicit dynamic code should exhibit a significant reduction in CPU time.

Acknowledgements

The work of M.B. Rubin was supported in part by visiting professorship at Centre des Matériaux, Mines ParisTech, France. Discussions with Prof. G. Cailletaud during the preparation of this manuscript are gratefully acknowledged.

Appendix A. Analytical solution for tension along [001]

An analytical solution of the SRIX model is provided in the case of a single crystal in simple tension along direction [001]. Isotropic elasticity is used for simplicity, with Young's modulus E and Poisson ratio ν. Hardening is not considered in the derivation so as to reach explicit expressions. The axial strain rate can be decomposed into elastic and plastic contributions as follows:

$$\dot{\varepsilon}_{33} = \dot{\varepsilon}^e_{33} + \dot{\varepsilon}^p_{33} = \frac{\dot{\sigma}_{33}}{E} + \frac{8\dot{\gamma}}{\sqrt{6}} = \frac{\dot{\sigma}_{33}}{E} + \frac{8}{\sqrt{6}}\dot{\varepsilon}'\left(\frac{\sigma_{33}\Big/\sqrt{6} - \tau_c}{R}\right) \tag{23}$$

The loading direction 3 coincides with the crystallographic direction [001]. Eight slip systems are known to be activated simultaneously for FCC crystals, with the same slip rate $\dot{\gamma}$ for all of them for symmetry reasons. The corresponding Schmid factor is $1/\sqrt{6}$. The flow rule (7) has been used to compute the axial plastic strain rate. The equivalent deviatoric strain rate follows from Eq. (8):

$$\dot{\varepsilon} = \frac{2}{3}(\dot{\varepsilon}_{33} - \dot{\varepsilon}_{11}) \tag{24}$$

Another relation between the axial and lateral strain rate follows from the elastic volumetric change:

$$2\dot{\varepsilon}_{11} + \dot{\varepsilon}_{33} = \frac{\dot{\sigma}_{33}}{E}(1 - 2\nu) \tag{25}$$

Combining Eqs. (23) and (25), a differential equation is obtained for the stress as a function of strain:

$$E\dot{\varepsilon}_{33}\left(1 + \frac{8}{\sqrt{6}}\frac{\tau_c}{R} - \frac{4}{3}\frac{\sigma_{33}}{R}\right) = \dot{\sigma}_{33}\left(1 + \frac{1-2\nu}{3}\left(\frac{8}{\sqrt{6}}\frac{\tau_c}{R} - \frac{4}{3}\frac{\sigma_{33}}{R}\right)\right) \tag{26}$$

whose solution is obtained in the form:

$$E\varepsilon_{33} = \frac{1-2\nu}{3}\left(\sigma_{33} - \frac{3R}{2}\frac{1+\nu}{1-2\nu}\log\left(\sqrt{6}\tau_c + \frac{3}{4}R - \sigma_{33}\right)\right) + (1+\nu)\left(\frac{2\sqrt{6}}{3}\tau_c + \frac{R}{2}\log\frac{3R}{4}\right) \tag{27}$$

The integration constant was settled by imposing that the strain at yield is $\sqrt{6}\tau_c/E$. The representation (27) is valid for $\sigma_{33} \geq \sqrt{6}\tau_c$, i.e. beyond the initial yield stress. The solution (27) shows that a limit stress exists

$$\sigma^{\infty}_{33} = \sqrt{6}\tau_c + \frac{3}{4}R \tag{28}$$

that affinely depends on the overstress parameter R. It is reached after an exponential-like stress evolution corresponding to the development of the overstress. The smooth nonlinear transition is clearly visible in Fig. 10 where a high value of parameter R was chosen.

References

Anand, L., Kothari, M., 1996. A computational procedure for rate-independent crystal plasticity. J. Mech. Phys. Solids 44, 525–558.
Arminjon, M., 1991. A regular form of the Schmid law. Application to the ambiguity problem. Textures Microstruct. 14–18, 1121–1128.
Bertram, A., 1999. An alternative approach to finite plasticity based on material isomorphisms. Int. J. Plast. 15, 353–374.
Besson, J., Cailletaud, G., Chaboche, J.L., Forest, S., Blétry, M., 2009. Non–Linear Mechanics of Materials. Series: Solid Mechanics and its Applications, vol. 167. Springer, ISBN 978-90-481-3355-0, p. 433.
Bishop, J., Hill, R., 1951. A theoretical derivation of the plastic properties of a polycrystalline face–centered metal. Philos. Mag. 42, 414–427.
Busso, E., Cailletaud, G., 2005. On the selection of active slip systems in crystal plasticity. Int. J. Plast. 21, 2212–2231.
Darrieulat, M., Piot, D., 1996. A method of generating analytical yield surfaces of crystalline materials. Int. J. Plast. 12, 575–610.
Einav, I., 2012. The unification of hypoplastic and elasto-plastic theories. Int. J. Solids Struct. 49, 1305–1315.
El Houdaigui, F., Forest, S., Gourgues, A.F., Jeulin, D., 2007. On the size of the representative volume element for isotropic elastic polycrystalline copper. In: Bai, Y., Z., Q., Wei, Y. (Eds.), IUTAM Symposium on Mechanical Behavior and Micromechanics of Nanostructured Materials. Springer, Beijing, China, pp. 171–180.
Fortunier, R., 1989. Dual potentials and extremum work principles in single-crystal plasticity. J. Mech. Phys. Solids 37, 779–790.
Franciosi, P., 1985. The concepts of latent hardening and strain hardening in metallic single crystals. Acta Mater. 33, 1601–1612.
Gambin, W., 1991. Crystal plasticity based on yield surfaces with rounded-off corners. Z. Angew. Math. Mech. 71, T265–T268.
Gambin, W., 1992. Refined analysis of elastic plastic crystals. Int. J. Solids Struct. 29, 2013–2021.
Gambin, W., Barlat, D., 1997. Modeling of deformation texture development based on rate independent crystal plasticity. Int. J. Plast. 13, 75–85.
Haupt, P., 2000. Continuum Mechanics and Theory of Materials. Springer Verlag.
Hollenstein, M., Jabareen, M., Rubin, M., 2013. Modeling a smooth elastic–inelastic transition with a strongly objective numerical integrator needing no iteration. Comput. Mech. 52, 649–667.
Hollenstein, M., Jabareen, M., Rubin, M., 2015. Erratum to: modeling a smooth elastic–inelastic transition with a strongly objective numerical integrator needing no iteration. Comput. Mech. 55, 453. http://dx.doi.org/10.1007/s00466-014-1099-9.
Hutchinson, J., 1976. Bounds and self-consistent estimates for creep of polycrystalline materials. Proc. R. Soc. Lond. A348, 101–127.
Kocks, U., Argon, A., Ashby, M., 1975. Thermodynamics and Kinetics of Slip. Pergamon Press, Oxford, UK.
Lubliner, L., Taylor, R., Auricchio, F., 1993. A new model of generalized plasticity and its numerical implementation. Int. J. Solids Struct. 30, 3171–3184.
Malvern, L., 1951. The propagation of longitudinal waves of plastic deformation in a bar of material exhibiting a strain-rate effect. J. Appl. Mech. 18, 203–208.

Mandel, J., 1965. Généralisation de la théorie de plasticité de W.T. Koiter. Int. J. Solids Struct. 1, 273–295.
Mandel, J., 1973. Equations constitutives et directeurs dans les milieux plastiques et viscoplastiques. Int. J. Solids Struct. 9, 725–740.
Méric, L., Cailletaud, G., 1991. Single crystal modeling for structural calculations. Part 2: finite element implementation. J. Eng. Mater. Technol. 113, 171–182.
Méric, L., Cailletaud, G., Gaspérini, M., 1993. FE calculations of copper bicrystal specimens submitted to tension-compression tests. Acta Metall. 42, 921–935.
Méric, L., Poubanne, P., Cailletaud, G., 1991. Single crystal modeling for structural calculations. Part 1: model presentation. J. Eng. Mater. Technol. 113, 162–170.
Miehe, C., Schroeder, J., Schotte, J., 1999. Computational homogenization analysis in finite plasticity simulation of texture development in polycrystalline materials. Comput. Methods Appl. Mech. Eng. 171, 387–418.
Montheillet, F., Gilormini, P., Jonas, J., 1985. Relation between axial stresses and texture development during torsion testing: a simplified theory. Acta Metall. 33, 705–717.
Musienko, A., Tatschl, A., Schmidegg, K., Kolednik, O., Pippan, R., Cailletaud, G., 2007. Three-dimensional finite element simulation of a polycrystalline copper specimen. Acta Mater. 55, 4121–4136.
Nouailhas, D., Cailletaud, G., 1995. Tension-torsion behavior of single-crystal superalloys – experiment and finite-element analysis. Int. J. Plast. 8, 451–470.
Patoor, E., Lagoudas, D., Entchev, P., Brinson, L., Gao, X., 2006. Shape memory alloys, part I: general properties and modeling of single crystals. Mech. Mater. 38, 391–429.
Paux, J., Morin, L., Brenner, R., Kondo, D., 2015. An approximate yield criterion for porous single crystals. Eur. J. Mech. A/solids 51, 1–10.
Perzyna, P., 1970. The constitutive equations for rate sensitive plastic materials. Q. Appl. Math. 20, 321–332.
Renouard, M., Wintenberger, M., 1976. Déformation homogène par glissements de dislocations de monocristaux de structure cubique faces centrées sous l'effet de contraintes et de déplacements imposés. C.R. Acad. Sc. Paris, Série B 283, 237–240.
Roters, F., Eisenlohr, P., Hantcherli, L., Tjahjanto, D., Bieler, T., Raabe, D., 2010. Overview of constitutive laws, kinematics, homogenization and multiscale methods in crystal plasticity finite-element modeling: theory, experiments, applications. Acta Mater. 58, 1152–1211.
Rubin, M., 1994. Plasticity theory formulated in terms of physically based microstructural variables – part I: theory. Int. J. Solids Struct. 31, 2615–2634.
Rubin, M., 2012. Removal of unphysical arbitrariness in constitutive equations for elastically anisotropic nonlinear elastic-viscoplastic solids. Int. J. Eng. Sci. 53, 38–45.
Sabnis, P.A., Forest, S., Arakere, N.K., Yastrebov, V., 2013. Crystal plasticity analysis of cylindrical indentation on a ni-base single crystal superalloy. Int. J. Plast. 51, 200–213.
Sabnis, P.A., Mazière, M., Forest, S., Arakere, N.K., Ebrahimi, F., 2012. Effect of secondary orientation on notch–tip plasticity in superalloy single crystals. Int. J. Plast. 28, 102–123.
Schurig, M., Bertram, A., 2003. A rate independent approach to crystal plasticity with a power law. Comput. Mater. Sci. 26, 154–158.
Šiška, F., Forest, S., Gumbsch, P., 2007a. Simulation of stress–strain heterogeneities in copper thin films: texture and substrate effects. Comput. Mater. Sci. 39, 137–141.
Šiška, F., Forest, S., Gumbsch, P., Weygand, D., 2007b. Finite element simulations of the cyclic elastoplastic behavior of copper thin films. Model. Simul. Mater. Sci. Eng. 15, S217–S238.
Šiška, F., Weygand, D., Forest, S., Gumbsch, P., 2009. Comparison of mechanical behaviour of thin film simulated by discrete dislocation dynamics and continuum crystal plasticity. Comput. Mater. Sci. 45, 793–799.
Vattré, A., Devincre, B., Roos, A., 2010. Orientation dependence of plastic deformation in nickel-based single crystal superalloys: discretecontinuous model simulations. Acta Mater. 58, 1938–1951.
Z–set package, 2013. Non-linear Material & Structure Analysis Suite. www.zset-software.com.